Journal of Structural Biology **130,** 34–44 (2000)
doi:10.1006/jsbi.2000.4236, available online at http://www.idealibrary.com on IDEAL®

Plasmodium falciparum-Infected Erythrocytes: Qualitative and Quantitative Analyses of Parasite-Induced Knobs by Atomic Force Microscopy

Eriko Nagao, Osamu Kaneko, and James A. Dvorak

Laboratory of Parasitic Diseases, National Institute of Allergy and Infectious Diseases, National Institutes of Health, Bethesda, Maryland 20892-0425

Received November 29, 1999, and in revised form February 1, 2000

We used the combination of an atomic force microscope and a light microscope equipped with epifluorescence to serially image *Plasmodium falciparum*-infected erythrocytes. This procedure allowed us to determine unambiguously the presence and developmental stage of the malaria parasite as well as the number and size of knobs in singly, doubly, and triply infected erythrocytes. Knobs are not present during the ring stage of a malaria infection but a lesion resulting from invasion by a merozoite is clearly visible on the erythrocyte surface. This lesion is visible into the late trophozoite stage of infection. Knobs begin to form during the early trophozoite stage of infection and have a single-unit structure. Our data suggest the possibility that a two-unit structure of knobs, which was reported by Aikawa *et al.* (1996, *Exp. Parasitol.* 84, 339–343) using atomic force microscopy, appears to be a double-tipped image. The number of knobs per unit of host cell surface area is directly proportional to parasite number in both early and late trophozoite stages. These results indicate that knob formation by one parasite does not influence knob formation by other parasites in a multiply infected erythrocyte. In addition, knob volume is not influenced by either parasite stage or number at the late trophozoite stage, indicating that the number of component molecules per knob is constant throughout the parasite maturation process.

Key Words: **atomic force microscopy; tapping mode; erythrocyte; knob; malaria; *Plasmodium falciparum*.**

INTRODUCTION

One of the hallmarks of a *Plasmodium falciparum* infection is the development of protrusions on the surface of infected erythrocytes. These protrusions or knobs mediate the adherence of infected erythrocytes to the endothelial cells lining cerebral blood vessels, resulting in potentially fatal cerebral complications (MacPherson *et al.*, 1985). The major aspects of the adhesion process have been elucidated. Knob components are synthesized by the parasite and transported to the erythrocyte membrane via Maurer's clefts, inducing knob formation (Aikawa *et al.*, 1986; Howard *et al.*, 1987). Following transport to the erythrocyte membrane, a knob-associated histidine-rich protein (KAHRP) and *P. falciparum* erythrocyte membrane protein 2 (PfEMP2), a structural knob protein, interact with several erythrocyte membrane molecules as well as *P. falciparum* erythrocyte membrane protein 1 (PfEMP1), a knob surface protein, to produce functional knobs. Finally, functional knobs interact with endothelial cell surface molecules (e.g., CD36, ICAM-1, and thrombospondin) through receptor–ligand binding (reviewed by Deitsch and Wellems (1996)).

Langreth *et al.* (1978) reported that by transmission electron microscopy (TEM) trophozoite-stage knobs appeared to be smaller in diameter and more dense than schizont-stage knobs. In contrast, Gruenberg *et al.* (1983) reported in scanning electron microscopy (SEM) studies that trophozoite-stage knobs appeared to be larger in diameter and less dense than schizont-stage knobs. However, the TEM study was based, by necessity, on a very limited number of ultrathin sections, which makes it prone to sampling errors. The SEM study was hampered by an inability to identify the number or stage of the infecting parasites. Recently, atomic force microscopy (AFM) studies of knobs on *P. falciparum*-infected erythrocytes demonstrated an apparent two-subunit knob structure with a uniform orientation of the subunits (Aikawa *et al.*, 1996; Aikawa, 1997; Nakano and Aikawa, 1998).

A major problem with both SEM and AFM studies has been the inability to identify either the develop-

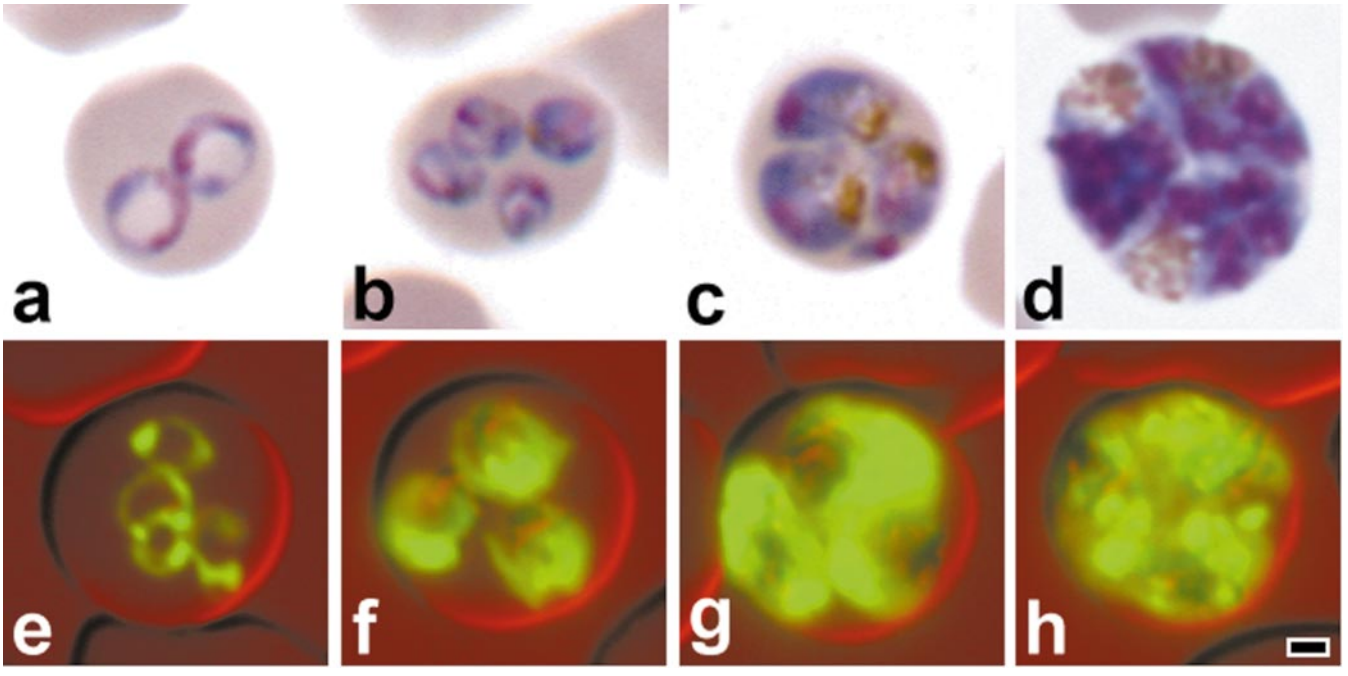

FIG. 1. Representative example of multiple *P. falciparum*-infected erythrocytes stained with Giemsa (top row) or YOYO (bottom row). (a, e) Ring stage. (b, f) Early trophozoite stage. (c, g) Late trophozoite stage. (d, h) Schizont stage. Bar represents 1 μm.

mental stage of the parasites or the number of parasites present in the erythrocyte. To overcome these problems, we used the fluorescent dye YOYO-1 iodide (YOYO), which stains both DNA and RNA, to identify *P. falciparum*-infected erythrocytes by light microscopy (LM) and, subsequently, used a coaxially mounted AFM to image the same erythrocytes. In this report we present the results of a study in which we were able to determine unambiguously the developmental stage of the parasite as well as the number and size of knobs in singly, doubly, and triply infected erythrocytes.

MATERIALS AND METHODS

P. falciparum *culture.* The *P. falciparum* ITO/A4 clone was used for this study (Roberts *et al.*, 1992). Parasites were grown as described by Trager and Jensen (1976) with the exception that a candle jar was not used; cultures were gassed with a mixture of 5% CO_2, 5% O_2, 90% N_2. Complete culture medium consisted of RPMI 1640 with L-glutamine without $NaHCO_3$ (Life Technologies, Baltimore, MD) supplemented with 25 mM Hepes (Calbiochem, San Diego, CA), 26.8 mM $NaHCO_3$ (Biofluids, Inc., Rockville, MD), 50 μg/ml hypoxanthine (Sigma, St. Louis, MO), 20 μg/ml gentamicin, and 5 mg/ml AlbuMAX I (Life Technologies) (Gerold *et al.*, 1996). Cultures were initiated with a mixture of freshly thawed, cryo-preserved parasites and fresh erythrocytes at a 2% hematocrit concentration in T75 culture flasks (Corning, Cambridge, MA) and incubated at 37°C.

Type O+ erythrocytes were used in place of type AB+ erythrocytes as described by Trager and Jensen (1976). The erythrocytes were washed twice with a minimum of 10 vol of culture medium without sodium bicarbonate, gentamicin, and AlbuMAX I and once with complete culture medium at room temperature (RT). Leukocytes were removed at each washing step by aspiration. The washed erythrocytes were suspended in complete culture medium at a 50% concentration, stored at 4°C, and used within 2 weeks.

AFM sample preparation. Erythrocytes infected with various stages of an unsynchronized *P. falciparum* culture (10% parasitemia) were diluted to 8.5×10^6 cells/ml with complete culture medium, and 200-μl portions were plated onto 22-mm-diameter coverglasses (Becton Dickinson Labware, Lincoln Park, NJ), which previously had been exposed to amylamine (Sigma) vapor for 2 min in a PLASMOD (Tegal Corp., Novato, CA) plasma generator. Erythrocytes were allowed to settle and attach to the surface of the amine-coated coverglass for 30 min at 37°C, after which the culture medium was carefully removed. The erythrocytes were fixed with osmium vapor for 2 min, washed with 0.1 M sodium cacodylate buffer (pH 7.4) (Electron Microscopy Sciences, Fort Washington, PA), fixed with 4% paraformaldehyde (Electron Microscopy Sciences) in 0.1 M sodium cacodylate buffer for 1 h at RT, washed, and stored in 0.1 M sodium cacodylate buffer at 4°C until processed for AFM imaging.

Parasites in infected erythrocytes were stained with 2.5 μM YOYO (Molecular Probes, Inc., Eugene, OR) in 0.1 M sodium cacodylate for 1 h at RT in a moist chamber, washed with deionized water, serially dehydrated for 5 min each with 30, 50, 70, 80, and 90% ethanol/water and finally absolute ethanol, and subsequently critical-point dried in a Polaron Model CPD7501 (VG Microtech, East Sussex, UK) critical-point dryer. In parallel LM experiments, infected erythrocytes were smeared on 1×3 in. microscope slides, dried, fixed with methanol, and stained with either Giemsa or YOYO.

AFM imaging and data collection. We used a Bioscope AFM (Digital Instruments, Santa Barbara, CA) attached to a Zeiss Axiovert 100 (Carl Zeiss, Thornwood, NY) inverted LM and a Nano-Scope III controller (Digital Instruments) as described previously (Nagao and Dvorak, 1998). Silicon nitride probes (Model TESP, Digital Instruments) on 125-μm-long by 30- to 40-μm-wide single-beam cantilevers with a spring constant of 20–100 N/m and tuned to a frequency of 250–300 kHz were used to

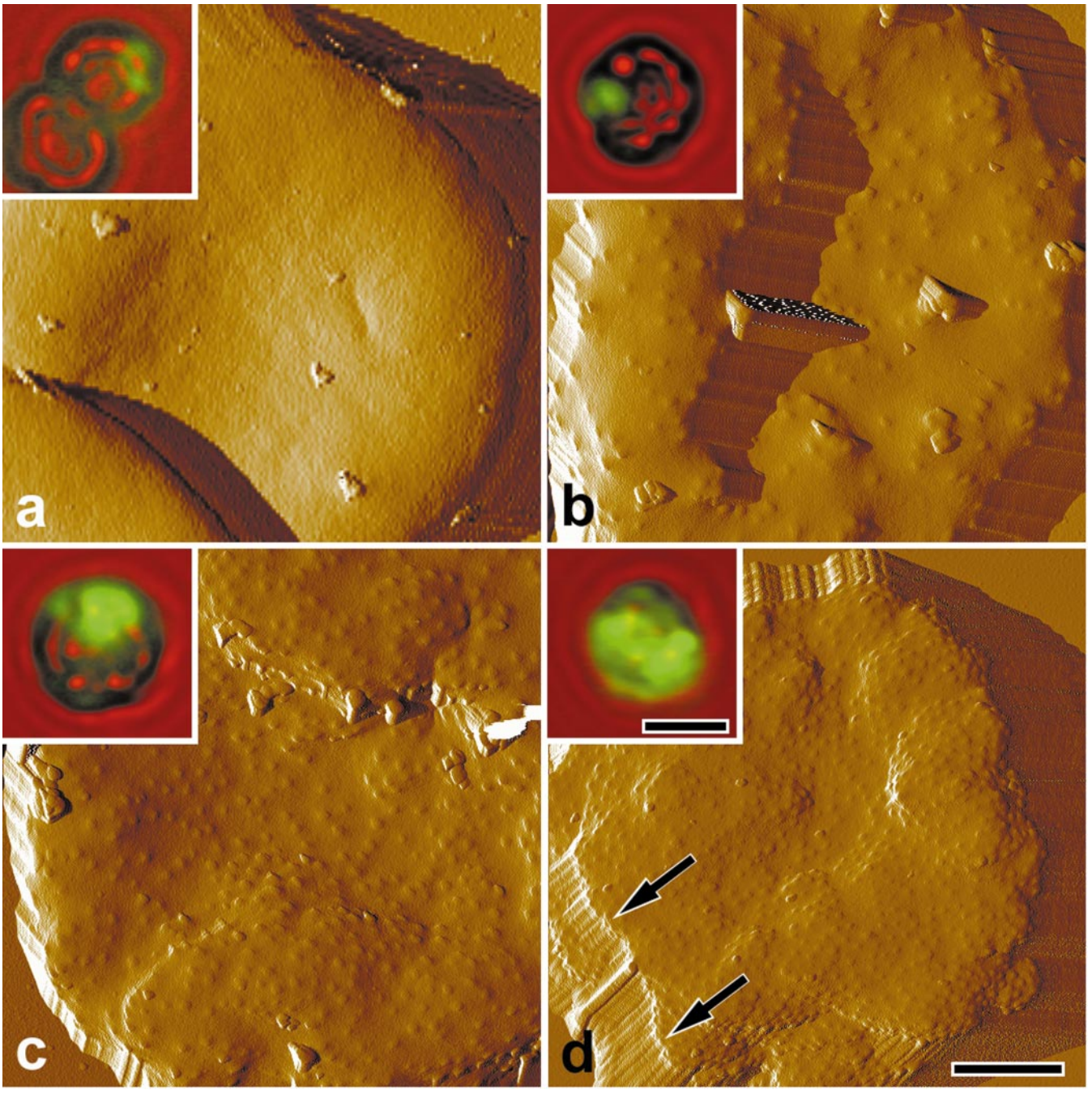

FIG. 2. AFM amplitude-mode images of single *P. falciparum*-infected erythrocytes at various developmental stages. The LM inset shows the same cell imaged with BF and epifluorescence microscopy prior to AFM scanning. (a) Ring stage. (b) Early trophozoite stage. (c) Late trophozoite stage. (d) Schizont stage. Arrows indicate a scanning artifact. Bars in (d) represent 1 μm for the AFM images and 5 μm for the LM inset images.

scan the cells. Topographic and amplitude (error signal) images were collected simultaneously at a scan rate of 0.5 Hz as 512 × 512 data arrays in the trace direction using tapping mode. All images were collected at a tapping force (A_{sp}/A_0) of 0.8 (Magonov *et al.*, 1997; Nagao and Dvorak, 1999). None of the images presented in this report were subjected to any form of image processing except Figs. 4a and 4b, which were plane-fitted and flattened and are represented as three-dimensional images.

LM imaging and data collection. Bright-field (BF) and YOYO-induced fluorescence images were collected from infected erythrocytes with a Zeiss Plan APOCHROMAT 20×/0.75 objective, a 4× projector and a chilled CCD video camera (Model C5985, Hamamatsu Photonic Systems, Bridgewater, NJ) prior to AFM scanning. BF images consisted of a single video frame; fluorescence images obtained with the Zeiss 487917 filter set were produced by integrating the video signal for 450 video frames. All images were

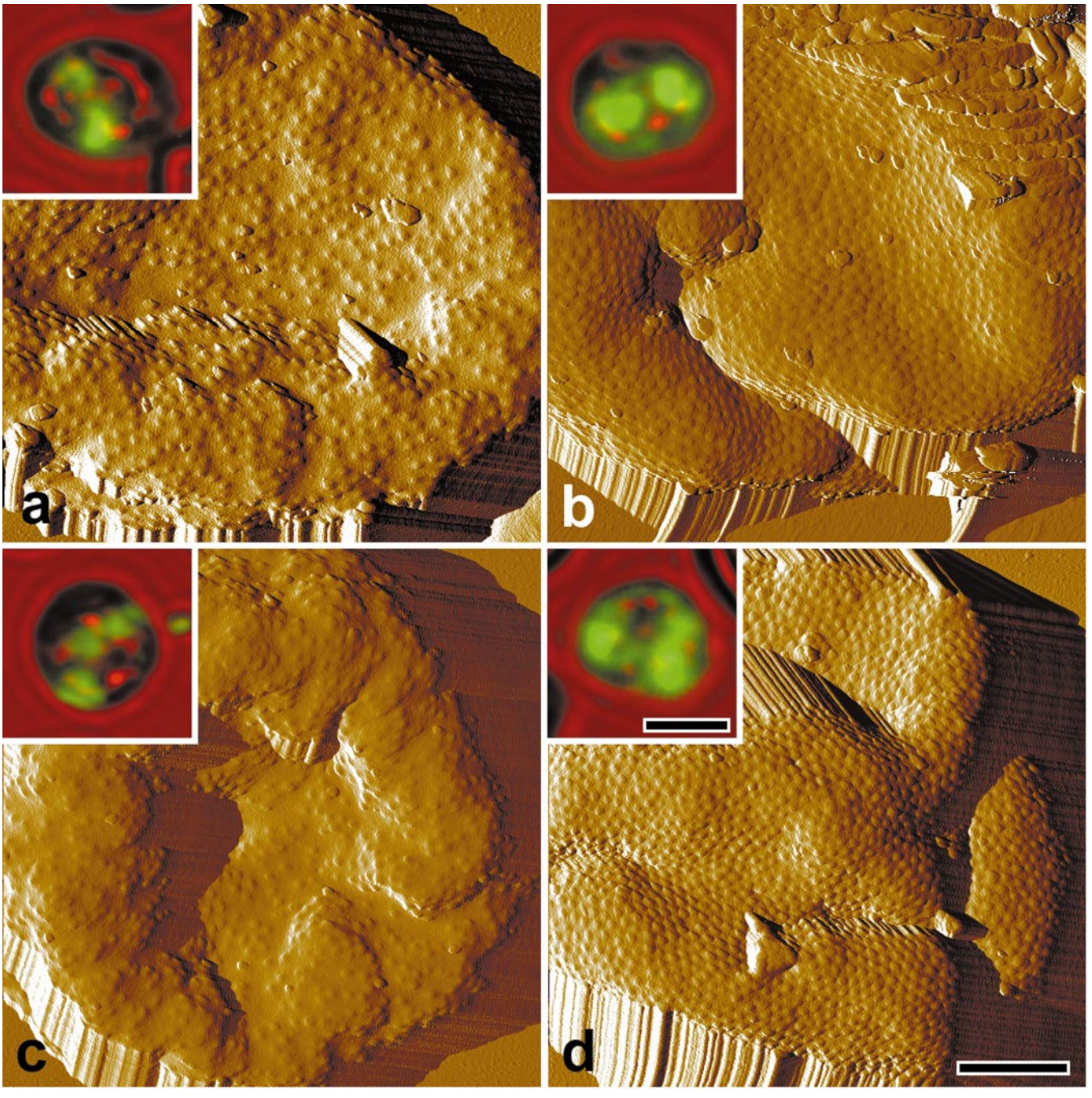

FIG. 3. AFM amplitude-mode images of double and triple *P. falciparum*-infected erythrocytes at early and late trophozoite developmental stages. The LM inset shows the same cell imaged by the BF and epifluorescence microscopy prior to AFM scanning. (a) Early trophozoite stage doubly infected erythrocyte. (b) Late trophozoite stage doubly infected erythrocyte. (c) Early trophozoite triply infected erythrocyte. (d) Late trophozoite stage triply infected erythrocyte. Bars in (d) represent 1 μm for the AFM images and 5 μm for the LM inset images.

imprinted with a digital time and date stamp (Model VTG-33, FOR.A Co., Ltd., Japan), passed into a DT3155 video frame grabber (Data Translation, Marlboro, MA) in a 400 MHZ Pentium II PC operating under Windows NT 4.0 workstation, service pack 4, and captured with Image-Pro Plus version 4 (Media Cybernetics, Silver Spring, MD).

Differential interference contrast and YOYO-stained fluorescence images of erythrocytes and color images of Giemsa-stained erythrocytes were collected using a chilled CCD digital camera (Model C4742-95, Hamamatsu Photonic Systems) attached to a Zeiss Axiophot as described above except that a Plan APOCHROMAT 100×/1.4 objective and an IC-PCI frame grabber (Imaging Technology, Bedford, MA) were used to capture the images. Three transmitted-light, monochrome images of Giemsa-stained speci-

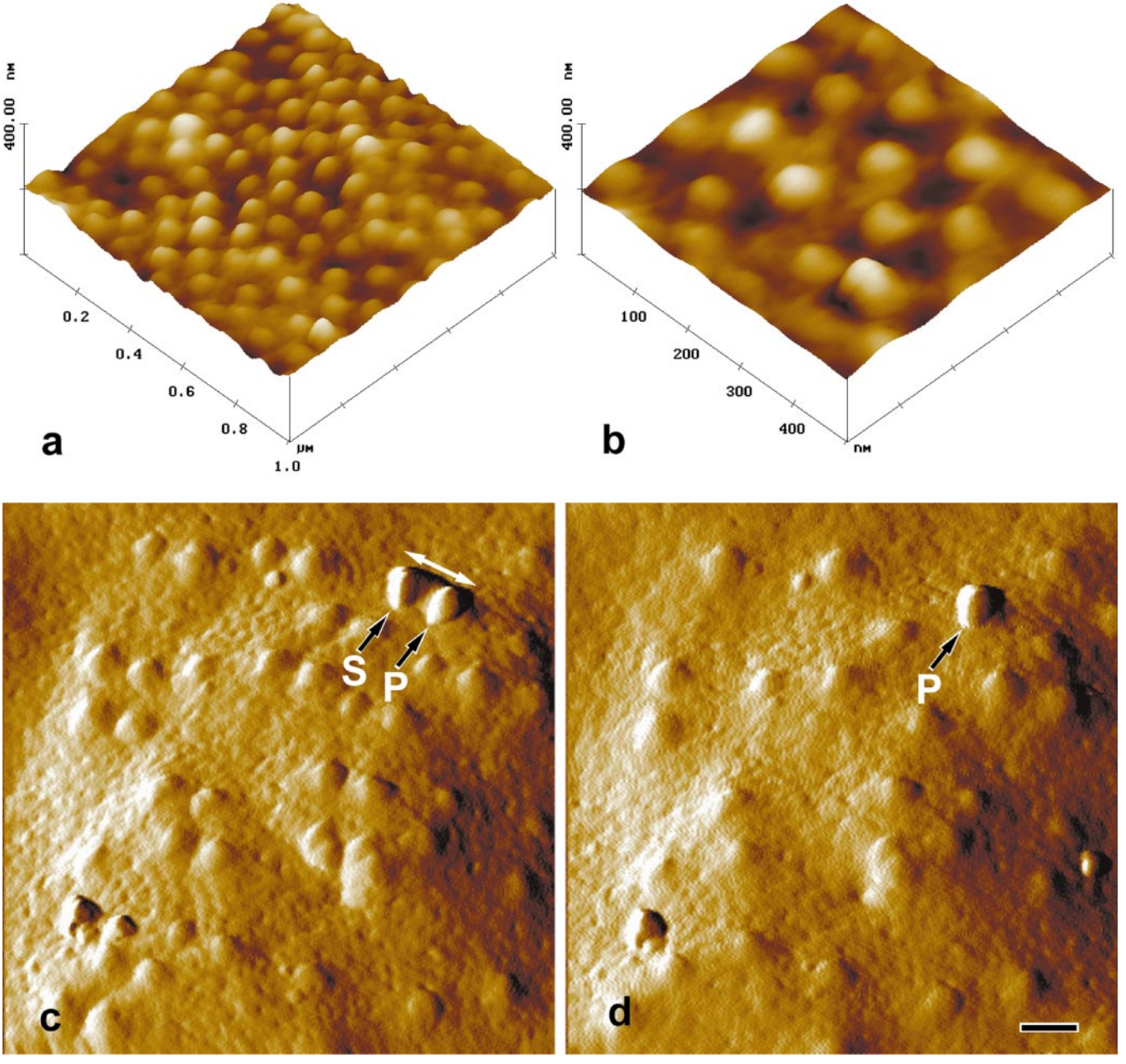

FIG. 4. Three-dimensional representation (a, b) of AFM height mode images of a late trophozoite stage *P. falciparum*-infected erythrocyte and AFM amplitude images of early trophozoite stage *P. falciparum*-infected erythrocytes imaged with a known double-tipped probe (c) and a single-tipped probe (d). Arrows in (c) indicate the direction of the second image orientation. The bar in (d) represents 0.2 μm.

mens were made using red, green, and blue color filters. The monochrome image files were merged in Image-Pro Plus to produce true color images.

RESULTS

Identification of Infected Erythrocytes

We tried many dyes (Giemsa, Hoechst 33258, DAPI, acridine orange, propidium iodide, and YOYO) to stain infected erythrocytes and found that only the fluorescent dye YOYO survived the subsequent dehydration and critical-point drying steps required for combined fluorescence and AFM studies. Figure 1 shows a comparison of conventional Giemsa (Figs. 1a, 1b, 1c, and 1d) to YOYO (Figs. 1e, 1f, 1g, and 1h) staining of multiply infected erythrocytes at various stages of development. We could identify infected

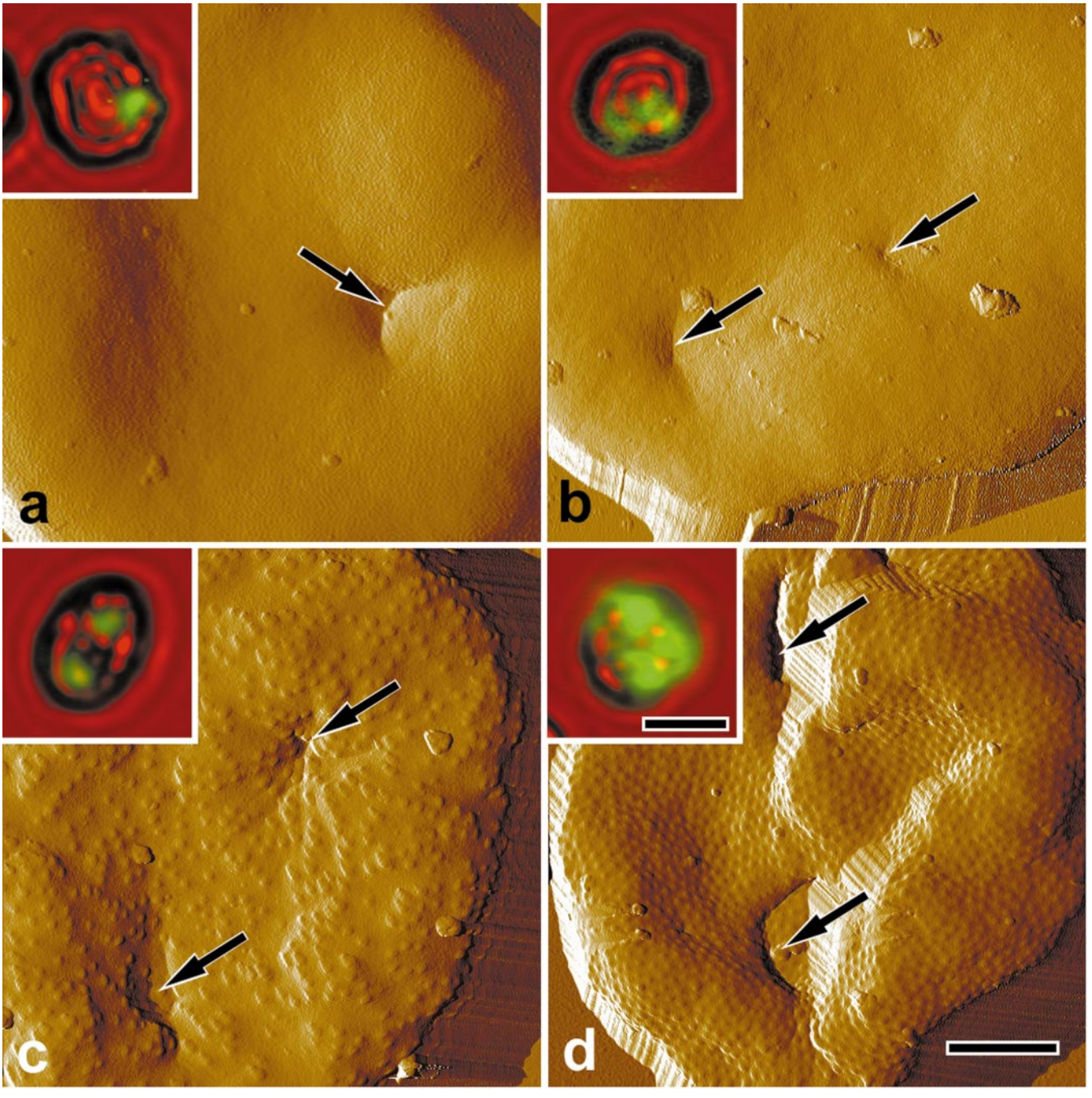

FIG. 5. AFM amplitude-mode images of *P. falciparum*-infected erythrocytes. The LM inset shows the same cell imaged by BF and epifluorescence microscopy prior to AFM scanning. (a) Posterior end of merozoite (arrow) in the process of invading an erythrocyte. (b) Two lesions (arrows) resulting from infection of an erythrocyte by two parasites that have progressed to the ring stage of development. (c) Two lesions (arrows) resulting from infection of erythrocyte by two parasites that have progressed to the early trophozoite stage of development. (d) Triple infected erythrocyte at a late trophozoite stage. Two lesions (arrows) resulting from infection of the erythrocyte by merozoites are clearly visible; a third lesion was not unambiguously identifiable. Bars in (d) represent 1 μm in the AFM images and 5 μm for the LM inset images.

cells by developmental stage, parasite number, and position of the malaria parasite within an erythrocyte as readily by YOYO staining as by conventional Giemsa staining. We divided the trophozoite stage of development into an early trophozoite stage where the parasites are relatively small (Figs. 1b and 1f) and a late trophozoite stage where the parasites are markedly larger (Figs. 1c and 1g). Merozoite nuclei and unstained residual bodies were observed clearly at the schizont stage of development (Figs. 1d and 1h).

AFM Images of Infected Erythrocytes

Infected erythrocytes at various stages of development (Fig. 2) were identified by fluorescence LM and scanned by AFM. Topographic AFM images showed that knobs were not present on the surface of ring stage-infected erythrocytes (Fig. 2a). Knobs, in the form of small protrusions on the surface of erythrocytes, began to appear on the surface of early trophozoite stage-infected erythrocytes (Fig. 2b) and became more numerous on the surface of late trophozoite stage-infected erythrocytes (Fig. 2c). Moreover, by the schizont stage of development (Fig. 2d), the number of knobs is markedly greater than found on all previous developmental stages. The circumferential edges of erythrocytes show a scanning artifact (Fig. 2d, arrows). This unavoidable artifact, a consequence of erythrocyte thickness, is due to imaging with the side walls of the pyramid-shaped probe rather than the probe tip.

Figures 3a and 3b show LM fluorescence and topographic AFM images of doubly infected erythrocytes at early and late trophozoite stages. Knob density on the surface of doubly infected erythrocytes at both early and late trophozoite stages is qualitatively higher than on equivalent stages of singly infected erythrocytes (Figs. 2b and 2c). Figures 3c and 3d show triply infected erythrocytes containing early and late trophozoite stage parasites. Again, knob density on the surface of triply infected erythrocytes at both early and late trophozoite stages is markedly higher than on doubly infected erythrocytes at the same stages. The late trophozoite stage-infected erythrocyte surface (Fig. 3d) was imaged at increasing magnifications and is represented as three-dimensional images (Figs. 4a and 4b). Knobs appeared as uniformly distributed, single-unit structures with no apparent preferred orientation.

As we were unable to duplicate the previously reported two-subunit knob structure reported in earlier AFM studies (Aikawa *et al.*, 1996; Aikawa, 1997; Nakano and Aikawa, 1998), we investigated the possible cause of this discrepancy. To test whether a multiple-tipped AFM probe could be responsible for the previously reported two subunit structure of parasite-induced knobs, we scanned the surface of an infected erythrocyte with a known double-tipped probe and the identical region with a single-tipped probe. A two-subunit knob structure was observed when we used a double-tipped probe (Fig. 4c), and the structures were all oriented in the same direction (arrows), a hallmark of a double-tipped probe-produced image. When the same area of the cell was scanned with a single-tipped probe (Fig. 4d), the knobs presented a single-unit structure with no apparent orientation direction.

The invasion of erythrocytes by merozoites and the lesions resulting from invasion of erythrocytes by merozoites can be observed by AFM when the parasite invades the concave surface of the erythrocyte. Figure 5a shows a merozoite in the process of invading an erythrocyte. The posterior end of the merozoite (arrow) is clearly visible. Two lesions (Fig. 5b, arrows) are present on the surface of an erythrocyte infected with two ring-stage parasites. Remarkably, lesions resulting from merozoite invasion are still visible at early and late trophozoite developmental stages (Figs. 5c and 5d, arrows).

Quantitative Analyses of Knob Number and Size

Knob height and volume were quantified with respect to both parasite developmental stage and the number of parasites per erythrocyte. Knobs ranged in height from 18.2 to 25.3 nm and have elliptical cross-sectional geometry with an eccentricity ratio varying between 0.85 and 0.91. The number of knobs per square micrometer increased approximately two-fold between early and late trophozoite stages and between late trophozoite and schizont stages (Fig. 6a). Both ellipticity and height were essentially constant during maturation of the parasite within the erythrocyte. Knob volume was calculated assuming it to be an elliptical cylinder. In contrast to knob density, knob volume did not vary as a function of parasite developmental stage (Table I).

Both knob number and volume were also quantified in relation to the number of intracellular parasites at both early and late trophozoite stages. There is a linear, parasite stage-independent relationship between the number of knobs per square micrometer and the number of parasites per erythrocyte (Fig. 6b). However, as shown in Fig. 7, knob volume is inversely proportional to the number of parasites per erythrocyte at the early trophozoite stage, but independent of parasite number at the late trophozoite stage.

DISCUSSION

Gruenberg *et al.* (1983) purified partially synchronized *P. falciparum*-infected erythrocyte cultures by density gradient-centrifugation procedures, imaged the cells by SEM, and quantified knob size and

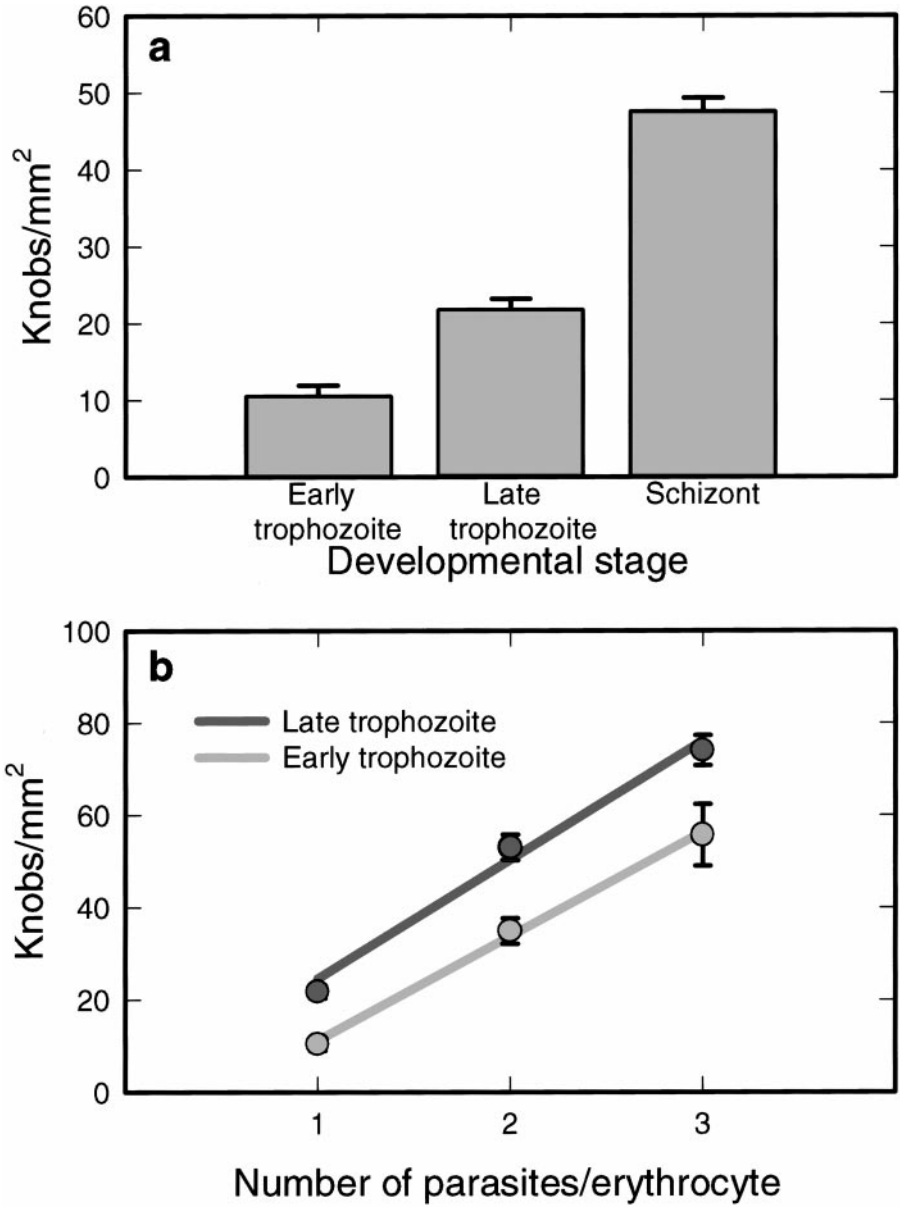

FIG. 6. Graphical representation of knob density (a) on singly *P. falciparum*-infected erythrocytes at the early trophozoite, late trophozoite, and schizont stages of development and (b) on *P. falciparum* singly, doubly, and triply infected erythrocytes during early and late trophozoite stages of development. Data in both graphs are expressed as means ± SEM for five infected erythrocytes. The regression for early trophozoite stage parasites (knobs/μm^2 = 22.5 × parasites/erythrocyte − 11.4) is similar to the regression for late trophozoite stage data (knobs/μm^2 = 25.7 × parasites/erythrocyte − 1.2) in (b).

number. They concluded that ". . .It is impossible to precisely determine the stage of parasite development for an individual cell since no information regarding the parasite itself can be obtained using the present procedures. It is also impossible to ascertain what (if any) the effects of multiple infection were on knob production in a single erythrocyte. . . ." One advantage of the Bioscope AFM is the ability to use it in combination with LM modalities to unambiguously identify the number and stage of the malaria parasites. We applied this technique to overcome the problems and limitations inherent in both TEM and SEM studies of *P. falciparum*-infected erythrocytes.

Our data clearly demonstrate that knobs begin to appear on the surface of infected erythrocytes at the early trophozoite stage of development and increase in number continuously throughout the maturation process. We also demonstrate that the number of knobs present on the erythrocyte surface is directly proportional to the number of parasites that have infected the erythrocyte. This phenomenon is inde-

TABLE I

Values for the Ratio of Major to Minor Axes, Height, and Volume of Knobs on *P. falciparum* Singly, Doubly, and Triply Infected Erythrocytes at Various Stages of Development

Developmental stage	No. of parasites/ cell	Knob eccentricity ratio	Height (nm)	Volume ($nm^3 \times 10^3$)
Early trophozoite	1	1.096	23.41 ± 0.97	553
Late trophozoite	1	1.109	22.70 ± 0.85	534
Schizont	1	1.110	25.30 ± 0.96	533
Early trophozoite	2	1.110	21.70 ± 0.92	479
Late trophozoite	2	1.173	19.90 ± 1.05	379
Early trophozoite	3	1.136	18.20 ± 0.85	347
Late trophozoite	3	1.181	21.50 ± 1.30	518

Note. Height values are expressed as means ± SEM for approximately 20 samples. The eccentricity ratio of major vs minor axes was tested for significance between groups by Student's *t* test. No significant differences were found ($P > 0.05$).

pendent of parasite stage and is the first demonstration of a direct relationship between the number of knobs present on the surface of an erythrocyte and the number of *P. falciparum* parasites infecting the erythrocyte. These results indicate that the knob formation by one parasite does not influence knob formation by other parasites in a multiply infected erythrocyte. In addition, knobs are distributed uniformly over the surface of the erythrocyte irrespective of the developmental stage of the parasite or the number of parasites in an erythrocyte. In contrast to Gruenberg *et al.* (1983), who reported that knobs appeared to be present at a higher density on the surface of erythrocyte protuberances, we found that knob distribution was independent of erythrocyte surface topography. These data fortify the concept that although knob component proteins may be transported randomly to the erythrocyte membrane, knobs are formed along the erythrocyte membrane proteins (e.g., actin, band 4.1) that are in the junctional network complex underlying the erythrocyte membrane (Kilejian *et al.*, 1991; Lustigman *et al.*, 1990). This premise gains credence from the fact that individual knobs maintain a constant appearance

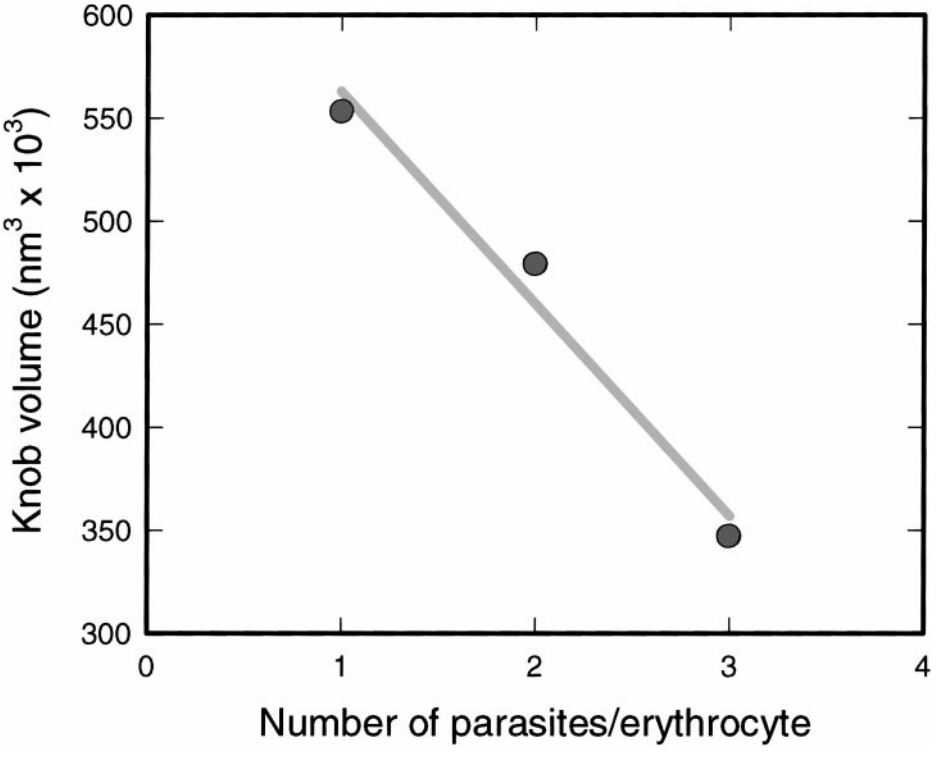

FIG. 7. Graphical representation of knob volume on *P. falciparum* singly, doubly, and triply infected erythrocytes at the early trophozoite stage of development. Knob volume ($nm^3 \times 10^3$) = $1.03 \times 10^5 \times$ parasites/erythrocyte − 6.65×10^5.

during the process of parasite maturation and do not coalesce, indicating that the number of component molecules per knob is constant throughout the parasite maturation process.

We used the unique ability of the AFM to provide topographic information to determine the height and major and minor axes of each knob. Aikawa (1988) reported in TEM studies that knobs are electron-dense conical protrusions with a height of 30–40 nm and a width of 90–100 nm in contrast to our estimates of a height of approximately 22 nm and a width of approximately 83 nm. This discrepancy may be a consequence of fixation or sampling error, which can result in quantitative analysis of thin sections. In this study, knob volume was not significantly influenced by either parasite stage or the number of late trophozoite stage parasites per erythrocyte. However, at the early trophozoite stage, knob volume was inversely related to parasite number. Decreases in both knob height and area contribute to this volume change. These observations may reflect marked metabolic changes occurring within the parasite during its intracellular development.

Our combined LM–AFM procedure also allowed us to determine the position of individual parasites within an erythrocyte and enables the new finding that lesions resulting from invasion by merozoites are clearly visible on the erythrocyte surface long after the invasion event has occurred. Although the presence of a parasitophorus duct in *P. falciparum*-infected erythrocytes was proposed by Pouvelle *et al.* (1991), the duct was suspected by others to be an *in vitro* artifact (Fujioka and Aikawa, 1993), and its existence is still controversial (Pouvelle and Gysin, 1997). The lesions we observed could be just scars on the erythrocyte surface resulting from merozoite invasion. However, it is also possible that the structures may represent an AFM demonstration of the terminus of a parasitophorus duct on the surface of the erythrocyte. Work is in process to resolve this issue by AFM-based analyses.

It is well known that AFM images produced using silicon nitride probes can often have a bipartite or double-image appearance (Hansma *et al.*, 1992). This phenomenon is due to the nature of the process used to produce the AFM probe. The silicon nitride probe is a crystal grown on the cantilever substrate. A large number of the crystals grown as AFM probes have more than one apex. When these probes are used for AFM imaging, a phenomenon known as double-tip imaging occurs. Hallmarks of double-tip imaging include image duplication with the secondary image of a structure being larger or smaller than the primary image depending upon the geometrical relationship between the two probe tips as well as the invariant relationship between the primary and the secondary images. We reproduced an oriented two-subunit structure of knobs using a known double-tipped probe and single-knob structure images of the same erythrocyte surface using a single-tipped probe. These data indicate that the previously reported aligned, two-subunit structure is the consequence of imaging with a double-tipped probe.

Our AFM study on *P. falciparum*-infected erythrocytes is a new and unique approach to malaria research, in general, and has the potential to develop as a useful tool for studies of other medically important host–parasite interactions.

The authors thank Carol C. Cunnick, Laboratory of Parasitic Diseases, NIAID, for her expert technical assistance.

REFERENCES

Aikawa, M. (1988) Human cerebral malaria, *Am. J. Trop. Med. Hyg.* **39,** 3–10.

Aikawa, M. (1997) Studies on *falciparum* malaria with atomic-force and surface-potential microscopes, *Ann. Trop. Med. Parasitol.* **91,** 689–692.

Aikawa, M., Uni, Y., Andrutis, A. T., and Howard, R. J. (1986) Membrane-associated electron-dense material of the asexual stages of *Plasmodium falciparum:* Evidence for movement from the intracellular parasite to the erythrocyte membrane, *Am. J. Trop. Med. Hyg.* **35,** 30–36.

Aikawa, M., Kamanura, K., Shiraishi, S., Matsumoto, Y., Arwati, H., Torii, M., Ito, Y., Takeuchi, T., and Tandler, B. (1996) Membrane knobs of unfixed *Plasmodium falciparum* infected erythrocytes: New findings as revealed by atomic force microscopy and surface potential spectroscopy, *Exp. Parasitol.* **84,** 339–343.

Deitsch, K. W., and Wellems, T. E. (1996) Membrane modifications in erythrocytes parasitized by *Plasmodium falciparum*, *Mol. Biochem. Parasitol.* **76,** 1–10.

Fujioka, H., and Aikawa, M. (1993) Morphological changes of clefts in *Plasmodium*-infected erythrocytes under adverse condition, *Exp. Parasitol.* **76,** 302–307.

Gerold, P., Schofield, L., Blackman, M. J., Holder, A. A., and Schwarz, R. T. (1996) Structural analysis of the glycosylphosphatidylinositol membrane anchor of the merozoite surface proteins-1 and -2 of *Plasmodium falciparum*, *Mol. Biochem. Parasitol.* **75,** 131–143.

Gruenberg, J., Allred, D. R., and Sherman, I. W. (1983) Scanning electron microscope-analysis of the protrusions (knobs) present on the surface of *Plasmodium falciparum*-infected erythrocytes, *J Cell Biol.* **97,** 795–802.

Hansma, H. G., Vesenka, J., Siegerist, C., Kelderman, G., Morrett, H., Sinsheimer, R. L., Elings, V., Bustamante, C., and Hansma, P. K. (1992) Reproducible imaging and dissection of plasmid DNA under liquid with the atomic force microscope, *Science* **256,** 1180–1184.

Howard, R. J., Uni, S., Lyon, J. A., Taylor, D. W., Daniel, W., and Aikawa, M. (1987) Export of *Plasmodium falciparum* proteins to the host erythrocyte membrane: Special problems of protein trafficking and topogenesis, *in* Chang, K.-P., and Snary, D. (Eds.), Host–Parasite Cellular and Molecular Interactions in Protozoal Infections, pp. 281–296. Springer-Verlag, New York.

Kilejian, A., Rashid, M. A., Aikawa, M., Aji, T., and Yang, Y.-F. (1991) Selective association of a fragment of the knob protein with spectrin, actin and the red cell membrane, *Mol. Biochem. Parasitol.* **44,** 175–182.

Langreth, S. G., Jensen, J. B., Reese, R. T., and Trager, W. (1978) Fine structure of human malaria in vitro, *J. Protozool.* **25,** 443–452.

Lustigman, S., Anders, R. F., Brown, G. V., and Coppel, R. L. (1990) The mature-parasite-infected erythrocyte surface antigen (MESA) of *Plasmodium falciparum* associates with the erythrocyte membrane skeletal protein, band 4.1, *Mol. Biochem. Parasitol.* **38,** 261–270.

MacPherson, G. G., Warrell, M. J., White, N. J., Looareesuwan, S., and Warrell, D. A. (1985) Human cerebral malaria. A quantitative ultrastructural analysis of parasitized erythrocyte sequestration, *Am. J. Pathol.* **119,** 385–401.

Magonov, S. N., Elings, V., and Whangbo, M.-H. (1997) Phase imaging and stiffness in tapping-mode atomic force microscopy, *Sur. Sci. Lett.* **375,** L385–391.

Nagao, E., and Dvorak, J. A. (1998) An integrated approach to the study of living cells by atomic force microscopy, *J. Microscopy* **191,** 8–19.

Nagao, E., and Dvorak, J. A. (1999) Phase imaging by atomic force microscopy: Analysis of living homoiothermic vertebrate cells, *Biophys. J.* **76,** 3289–3297.

Nakano, Y., and Aikawa, M. (1998) Ultrastructure of celebral malaria-infected erythrocytes, *Electron Microsc.* **32,** 93–98.

Pouvelle, B., and Gysin, J. (1997) Presence of the parasitophorus duct in *Plasmodium falciparum* and *P. vivax* parasitized Saimiri monkey red blood cells, *Parasitol. Today* **13,** 357–361.

Pouvelle, B., Spiegel, R., Hsiao, L., Howard, R. J., Morris, R. L., Thomas, A. P., and Taraschi, T. F. (1991) Direct access to serum macromolecules by intraerythrocytic malaria parasites, *Nature* **353,** 73–75.

Roberts, D. J., Craig, A. G., Berendt, A. R., Pinches, R., Nash, G., Marsh, K., and Newbold, C. I. (1992) Rapid switching to multiple antigenic and adhesive phenotypes in malaria, *Nature* **357,** 689–92.

Trager, W., and Jensen, J. B. (1976) Human malaria parasites in continuous culture, *Science* **193,** 673–675.